Electron collisions with the BH_2 radical using the *R*-matrix method

Song Bin Zhang,[1] Jian Guo Wang,[2] R. K. Janev,[3] and Xiang Jun Chen[1]

[1]*Hefei National Laboratory for Physical Sciences at Microscale and Department of Modern Physics, University of Science and Technology of China, Hefei 230026, China*

[2]*Key Laboratory of Computational Physics, Institute of Applied Physics and Computational Mathematics, P. O. Box 8009, Beijing 100088, China*

[3]*Macedonian Academy of Sciences and Arts, P. O. Box 428, 1000 Skopje, Macedonia*

(Received 24 September 2010; revised manuscript received 11 November 2010; published 22 December 2010)

Differential, integral, and momentum-transfer cross sections for the rotationally elastic and inelastic scattering of electron by the BH_2 radical at low collision energies (0–8 eV) are reported in a 22-state molecular *R*-matrix method. The excitation cross sections from the ground $X\,^2A_1$ state to the first two excited states $^2B_1$ and $^4A_2$ are calculated as well, for incident electron energies from the respective thresholds up to 8 eV. Configuration-interaction wave functions are used to represent the target states which account for the correlation effects. Four shape and three Feshbach resonances are detected. The Born-closure approximation is applied for the elastic and dipole-allowed transitions to account for the $l > 4$ partial waves excluded from the *R*-matrix calculations.

DOI: 10.1103/PhysRevA.82.062711 PACS number(s): 34.80.Bm, 34.80.Gs

I. INTRODUCTION

In the 1967 experiment of Herzberg and Johns [1], they assigned the absorption spectrum in the flash photolysis of H_3BCO to the free BH_2 radical and determined quite accurately the geometrical structure of both the ground and first excited states of BH_2. No other experiments have been reported about this short-living radical since then. However, in the 1970s and 1990s several theoretical studies were carried out, devoted to the properties of the first two states of BH_2 [2–7]. No such work has been done for the higher excited states of this radical, except the one of Peric *et al.* [6]. The electron collision processes with the BH_2 molecule so far have not been studied at all.

The purpose of the present article is to undertake an *ab initio* study of the structural properties of BH_2 radical within the complete active space configuration interaction (CAS CI) model and to investigate the dynamics of the electron-BH_2 collision system by using the molecular *R*-matrix method [8,9] with a large configuration-interaction (CI) basis. In particular, the cross sections for rotationally elastic and inelastic processes, as well as those for excitation of the first two excited electronic states $^2B_1$ and $^4A_2$, will be calculated in the energy region below 8 eV. Besides the intrinsic scientific interest of these studies, their results are of interest for the kinetics of magnetic fusion edge plasmas, where the BH_2 radical is present as an important impurity generated by the plasma-vessel wall interaction processes.

The article is organized as follows. In the next section we present an outline of the molecular *R*-matrix method, in Sec. III we discuss the structural properties of BH_2 molecule and define the expansion basis for our *R*-matrix calculations, while in Sec. IV we present our results for the studied collision processes. Section V gives a summary of the work. Atomic units will be used throughout this article, unless otherwise explicitly stated.

II. OUTLINE OF THE MOLECULAR *R*-MATRIX METHOD

The *R*-matrix theory for electron-molecule interactions has been discussed in detail by Burke and Tennyson *et al.* [10–12], and here we will give only a brief description of it. The basic idea of *R*-matrix theory is to divide the coordinate space into two regions, an inner region and an outer region. The inner region is defined by a sphere centered at the molecular center of mass, while the spherical boundary is placed so that the inner region (0–15 a.u.) encloses the entire *N*-electron target wave function. Since the scattering electron is indistinguishable from the electrons of the target, the short-range, exchange, and correlation interactions between the scattering electron and target electrons are completely taken into account in this region. In the outer region, the electron exchange and correlation effects between the scattering electron and target electrons are neglected. The scattering electron then moves in the long-range local multipole potential of the target and single-center close-coupling expansion of the wave function is used [13].

In the inner region, the wave function of the $(N+1)$-electron system is expanded in a CI basis [10–12]

$$\psi_k^{N+1} = \widehat{\mathrm{A}} \sum_{ij} a_{ijk} \phi_i^N(\mathbf{x}_1, \ldots, \mathbf{x}_N) u_{ij}(\mathbf{x}_{N+1}) + \sum_i b_{ik} \chi_i^{N+1}(\mathbf{x}_1, \ldots, \mathbf{x}_{N+1}), \quad (1)$$

where $\widehat{\mathrm{A}}$ is the antisymmetrization operator which accounts for the exchange between the target electrons and the scattering electron, $\mathbf{x}_N$ denotes the spatial and spin coordinates of the *N*-th electron, ϕ_i^N is the wave function of the *i*-th target state, u_{ij} are the extra orbitals introduced to represent the scattering electron, and χ_i^{N+1} are multicenter square-integrable (L^2) correlation functions. The summation in the first term in Eq. (1) generates the "target + continuum" configurations, while the second term involves configurations with no amplitude on the *R*-matrix boundary. This term allows for the high-angular-momentum effects in the region of nuclei and for the charge polarization effects [14] by placing the scattering electron into target occupied and virtual molecular orbitals. The variational parameters a_{ijk} and b_{ik} are obtained by diagonalization of the $(N+1)$-electron Hamiltonian matrix in the basis ${\psi_k}^{N+1}$.

TABLE I. Dominant configurations (with coefficient absolute value larger than 0.3), transition moments (in a.u.) (static dipole moment for the ground state), number of configurations (N), and vertical excitation energies (in eV) of the BH_2 radical.

State	Main configuration	Transition dipole moment (a.u.)		N	Vertical excitation energy (eV)		
					CAS	SD-CI	MRD CI[c]
$X\,^2A_1$	$2a_1^2 3a_1^1 1b_2^2$	0.1662	0.173[a] 0.142[b] 0.211[c]	3376	0.0	0.0	0.0
$^2B_1$	$2a_1^2 1b_1^1 1b_2^2$	0.2416	0.296[c]	3152	1.263	1.110	1.10 1.166[a]
$^4A_2$	$2a_1^2 3a_1^1 1b_1^1 1b_2^1$	0.000		2040	5.393	5.364	–
$^2A_1$	$2a_1^2 3a_1^1 1b_1^1 1b_2^1$	0.0677	0.657[c]	3376	6.253	6.230	5.54
$^2A_2$	$2a_1^2 3a_1^1 1b_1^1 1b_2^1$	0.0000	0.000[c]	3141	6.765	6.471	6.52
$^2B_2$	$2a_1^2 3a_1^2 1b_2^1$ $2a_1^2 1b_1^2 1b_2^1$	0.0699	0.059[c]	3344	7.307	6.706	6.41
$^2A_2$	$2a_1^2 3a_1^1 1b_1^1 1b_2^1$	0.000	0.000[c]	3141	7.454	7.212	7.15
$^2B_2$	$2a_1^2 1b_2^2 2b_2^1$ $2a_1^1 3a_1^1 1b_2^2 2b_2^1$	0.3982	0.084[c]	3344	7.565	7.548	6.62
$^4B_1$	$2a_1^1 3a_1^1 1b_1^1 1b_2^2$	0.000		2020	8.180	8.268	–
$^2A_1$	$2a_1^2 1b_2^2 2b_2^1$	0.0383	0.100[c]	3376	8.364	8.260	6.58
$^2B_2$	$2a_1^2 1b_2^2 2b_2^1$ $2a_1^2 1b_1^2 1b_2^1$	0.7229	0.563[c]	3344	8.369	8.300	7.17
$^2B_2$	$2a_1^2 1b_1^2 1b_2^1$ $2a_1^2 1b_1^1 2b_1^1 1b_2^1$ $2a_1^2 1b_2^2 2b_2^1$ $2a_1^2 3a_1^2 1b_2^1$	0.3887	0.356[c]	3344	8.881	8.736	8.40
$^2B_1$	$2a_1^2 1b_1^1 1b_2^2$	0.2866	0.111[c]	3152	9.680	9.585	6.67
$^2A_1$	$2a_1^2 3a_1^1 1b_2^2$	0.0006	0.172[c]	3376	9.845	9.596	7.03

[a]Staemmler *et al.* [3].
[b]Williams *et al.* [4].
[c]Perić *et al.* [6].

III. TARGET AND SCATTERING MODELS

The BH_2 radical belongs to the C_{2v} point group and possesses the experimental geometry with a B-H bond of 1.1801 Å and an angle H-B-H = 131.04° [15]. The ground state of BH_2 is designated as X^2A_1 and has the Hartree-Fock electronic configuration $1a_1^2 2a_1^2 1b_2^2 3a_1^1$. The double-zeta-plus-polarization Gaussian basis sets $(9s5p1d)/(4s2p1d)$ for B [16] and $(8s2p)/(5s2p)$ for H of Lie and Clementi [17] are used in the present calculations. We have not used diffuse functions in our basis as they would significantly extend outside the R-matrix sphere.

A restricted Hartree-Fock (RHF) calculation is performed at the experimental equilibrium geometry of the ground state of BH_2 radical that generates a set of occupied and virtual molecular orbitals (MO's). The HF energy of the target is −25.755 05 a.u., which compares quite well with our "all single and double" CI (SD CI) value −25.831 79 a.u.. The orbitals (and therefore orbital energies and Koopman's IP) from the RHF calculations are not uniquely defined (see Ref. [18] and references therein), so we do not show them here.

The CAS CI model is used to obtain the accurate transition moments and vertical excitation spectra of the excited states. In this model, two electrons are frozen to the core orbital $1a_1$, while five valence electrons are free to occupy the $2a_1, 3a_1, 4a_1, 5a_1, 6a_1, 7a_1, 1b_1, 2b_1, 1b_2, 2b_2, 3b_2, 4b_2$, and $1a_2$ MO's to produce the CAS. The vertical excitation energies (VEE) of the first 14 doublet and quartet excited states, transition dipole moments (static dipole moment for the ground state), dominant configurations, and the number of configurations for each state are presented in Table I. The present CAS values are compared with other theoretical results when available [3,4] and, in the case of VEE, with the results from our SD CI calculations. The present static dipole moment for the ground state is between the available theoretical results 0.142 a.u. [3] and 0.173 a.u. [4], 0.211 a.u. [6]. The VEE of the $^2B_1$ state from our CAS CI model is 1.263 eV and agrees very well with the CI results of Staemmler *et al.* [3] and Perić *et al.* [6], as well as with the result of our SD CI model. However, the CAS CI VEE values for the other excited states are higher by an amount within 0.3 eV than the values from our SD CI model, except for the first $^2B_2$ excited state for which the difference is 0.6 eV. It is possible to increase the account of correlations in our CAS CI model, and thereby to improve the VEE, but then the scattering calculations then could become intractable. It should be noted that in the MRD CI calculations

of Perić *et al.* [6], additional basis functions have been placed at the midpoints of the B-H bonds to produce more than 15 doublet valance and Rydberg states with excitation energies between 6.0 and 9.0 eV. We should also note that the first $^4A_2$ excited state with VEE 5.393 eV results from one electron in MO $1b_1$ excited to MO $1b_2$ from the ground state and interelectronic strong spin coupling. Table I also shows that the agreement between our results of those of Ref. [6] for the ground and the first two excited states is quite good. Our scattering calculations (see next section) will be, therefore, limited only to processes involving these three states.

No R-matrix pole in the $^1A_1$ scattering symmetry was found in the present calculations. However, such a pole has been found in the $^3B_1$ scattering symmetry with a vertical electron affinity of 0.142 eV, corresponding to a bound state of the anion BH_2^- with the $^3B_1$ symmetry, which agrees very well with the theoretical (adiabatic) result 0.16 eV [19]. The previous theoretical studies [19,20] predict BH_2 bound anions with both $^1A_1$ and $^3B_1$ symmetry, with a B-H bond of about 1.2 Å and H-B-H angles of about 102° and 126°, respectively. Since the present R-matrix calculations use the BH_2 equilibrium geometry with a much larger H-B-H angle than 102°, it is not surprising that no R-matrix pole with $^1A_1$ scattering symmetry was found.

The scattering calculations have been carried out by retaining 17 doublet states with the singlet A_1, A_2, B_1, and B_2 symmetries and 17 doublet + 5 quartet states with the triplet A_1, A_2, B_1, and B_2 symmetries in the expansion (1). All the target states are represented by CI wave functions and the states with VEE less than 10 eV are given in Table I (two $^2A_1$ and $^2B_2$, one $^2A_2, ^4A_1, ^4B_2$, and $^4A_2$ are not included in the table). The continuum orbitals of Faure *et al.* (Table II in Ref. [21]), represented by Gaussian-type orbitals (GTOs) centered at the molecular center of mass, have been used. Our calculations were performed for the continuum orbitals up to g partial waves. These continuum orbitals are orthogonalized to the target orbitals, and the continuum orbitals with an overlap of less than 2×10^{-7} were removed [22]. It is important to balance the correlations included in the target states and those in the scattering calculations. This is achieved by allowing six electrons (five valance electrons plus one scattering electron) to move freely among $2a_1, 3a_1, 4a_1, 5a_1, 6a_1, 7a_1, 1b_1, 2b_1, 1b_2, 2b_2, 3b_2, 4b_2$, and $1a_2$ molecular orbitals.

IV. RESULTS AND DISCUSSIONS

A. Differential cross sections

The evaluation of differential cross section (DCS) is a stringent test for any scattering theory. The DCS for a general polyatomic molecule is given by the following expression:

$$d\sigma/d\Omega = \sum_L A_L P_L(\cos\theta), \tag{2}$$

where P_L are the Legendre polynomials. The coefficients A_L have been discussed in detail by Gianturco and Jain [23]. For a polar molecule the expansion (2) over L converges slowly. To remedy this problem, one can use the following closure formula [24,25]:

$$d\sigma/d\Omega = d\sigma^B/d\Omega + \sum_L \left[A_L - A_L^B P_L(\cos\theta)\right]. \tag{3}$$

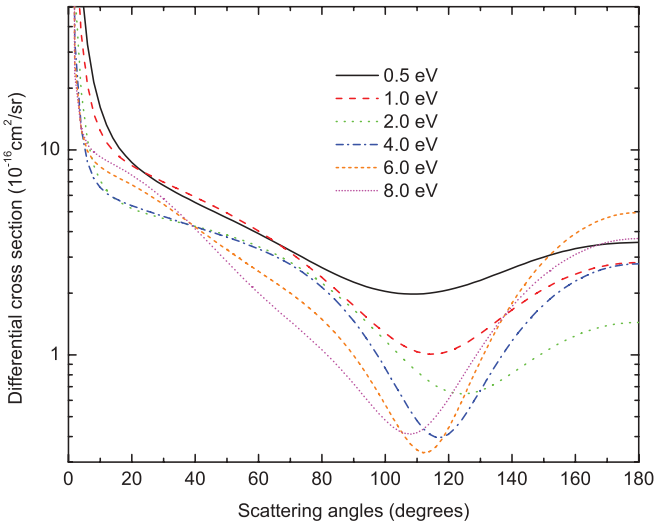

FIG. 1. (Color online) Differential elastic cross sections at different energies 0.5, 1.0, 2.0, 4.0, 6.0, and 8.0 eV.

The superscript B indicates that the relevant quantity is calculated by using the Born series with an electron-point dipole interaction. The summation over L in Eq. (3) now converges rapidly, since the contribution from the higher partial waves to the DCS is dominated by the electron-dipole interaction and can be calculated in the Born approximation. The quantity $d\sigma^B/d\Omega$ for any initial rotor state $|J\tau\rangle$ is given by the sum over all final rotor states $|J'\tau'\rangle$

$$\sigma^B/d\Omega = \sum_{J'\tau'} d\sigma^B/d\Omega(J\tau \to J'\tau'). \tag{4}$$

The expression for the state-to-state rotationally inelastic DCS, $d\sigma^B/d\Omega(J\tau \to J'\tau')$, for the spherical top, symmetric top, and asymmetric top molecules are given by Sanna and Gianturco [26].

The calculated dipole moment and rotational constants (6.169 320, 7.250 313, 41.378 161 cm^{-1}) at the equilibrium geometry are used to calculate the DCS in our 22-state close-coupling model in Table I. Figure 1 shows the present calculated DCS at the incident energies of 0.5, 1.0, 2.0, 4.0, 6.0, and 8.0 eV, which is obtained by summing up all the rotationally elastic and inelastic DCS with J up to 5 for each incident energy. The large cross sections in the forward direction are due to the dipolar nature of the target [27], and the state-resolved cross sections (discussed below) show that the pure elastic $(0 \to 0)$ transition is responsible for the appearance of the minimum in the summed cross section in the medium scattering angle region (80°–140°), which indicates the crucial role of the short-range interactions in the backward scattering region. To the best of our knowledge, experimental or theoretical DCS data for this molecule are still not available for comparison.

The state-resolved singlet and triplet cross sections at 1.0 eV are shown in Fig. 2. The $0 \to 1$ contribution is much smaller than the pure elastic $0 \to 0$ component except at very small angles, which results from the fact that BH_2 is a weakly dipolar molecule. The rotational elastic scattering $(0 \to 0)$ has the dominant contribution. The position of the backward-scattering minimum for the triplet component is larger than that for the singlet component by about 20°, whereas the dipole

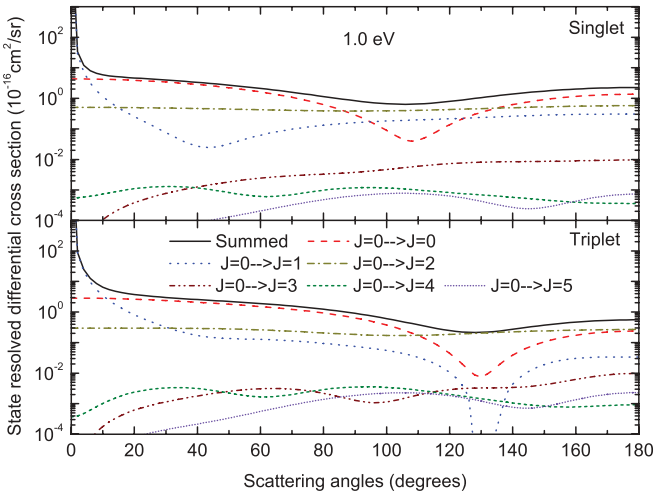

FIG. 2. (Color online) State-resolved differential cross sections at 1.0 eV.

component ($0 \rightarrow 1$) has the characteristic forward peak. The singlet and triplet components show forward and backward-scattering minima at about 40° and 130°, respectively. The quadrupolar component ($0 \rightarrow 2$) exhibits an almost flat behavior which is in conformity with the Born behavior. The cross-section contributions of $J > 2$ are negligible, thus ensuring that our DCS has converged with respect to the J value. We should note that with increasing the scattering energy, the contribution of the ($0 \rightarrow 4$) component becomes comparable to that of the ($0 \rightarrow 2$) component, and the position of backward-scattering minimum for the singlet ($0 \rightarrow 0$) component does not change, while that for the triplet ($0 \rightarrow 0$) component shifts closer to that of the singlet ($0 \rightarrow 0$) component.

B. Elastic integral and momentum transfer cross section

There are four IRs, A_1, A_2, B_1, and B_2, that contribute to the scattering process. Figure 3 shows the contributions of

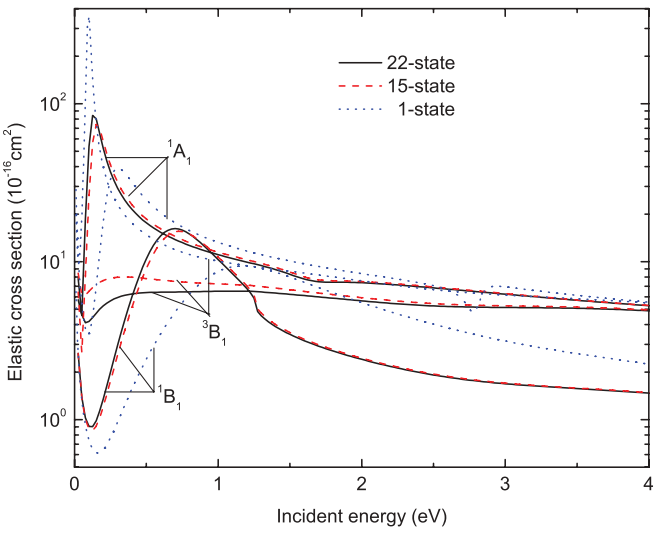

FIG. 3. (Color online) Elastic cross sections of the components $^1A_1, ^1B_1$, and $^3B_1$ for 1-state, 15-state and 22-state CI calculations in the energy range of 0–4 eV.

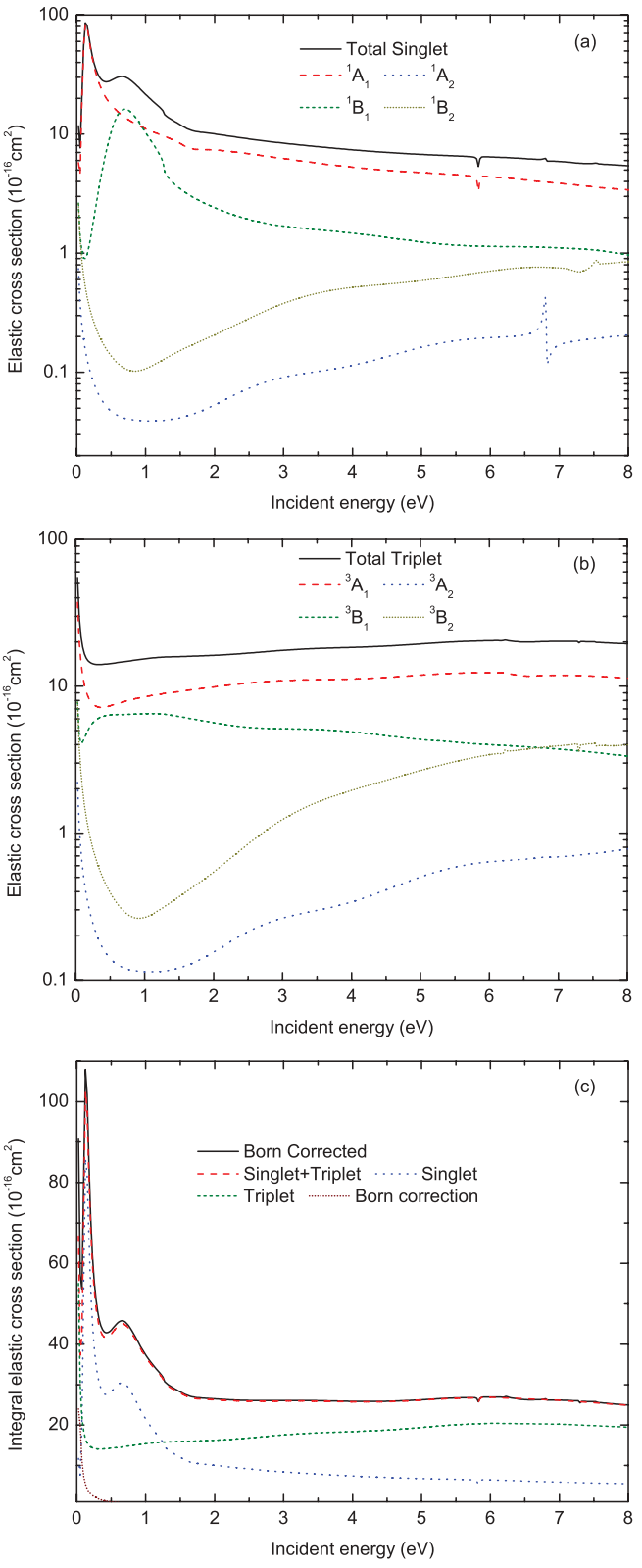

FIG. 4. (Color online) Elastic cross sections in the energy range of 0–8 eV. (a) Singlet A_1, A_2, B_1, and B_2 components and total singlet; (b) triplet A_1, A_2, B_1, and B_2 components and total triplet; (c) total singlet, total triplet, total singlet plus total triplet, Born correction, and Born corrected.

TABLE II. Resonant states of the electron-BH_2 scattering system.

			Resonance parameters (eV)		Parent state (eV)	
Sym	Designation of resonance	Type of resonance	Position/Er	Width/Γ	Sym	Position
$^1A_1$	$2a_1^2 3a_1^2 1b_2^2$	Shape	0.111	0.115	X^2A_1	0.0
$^1B_1$	$2a_1^2 3a_1^1 1b_1^1 1b_2^2$	Shape	0.614	0.619	X^2A_1	0.0
$^1A_1$	$2a_1^2 1b_1^2 1b_2^2$	Core-excited	1.628	0.691	$^2B_1$	1.263
$^3A_2$	$2a_1^2 3a_1^2 1b_1^1 1b_2^1$	Core-excited	5.962	0.517	$^4A_2$	5.393
$^1A_1$	$2a_1^2 3a_1^2 1b_2^2$	Feshbach	5.832	0.0240	$^2A_1$	6.253
$^3B_2$	$2a_1^2 3a_1^1 1b_2^2 2b_2^1$	Feshbach	6.203	0.0069	$^2A_1$	6.253
$^1A_2$	$2a_1^2 3a_1^2 1b_1^1 1b_2^1$	Feshbach	6.802	0.0291	$^2A_2$	7.454

$^1A_1, ^1B_1$, and $^3B_1$ to the elastic cross sections for 1-state, 15-state, and 22-state CI calculations. Clearly, one peak at 0.0947 eV is observed in the $^3B_1$ one-state component; however, this peak (or resonance) is not real, because it is converted into the $^3B_1$ bound anion described in Sec. III in the 22-state calculations due to the inclusion of higher excited states. The retention of a large number of electronic channels in the 22-state model provides the necessary polarization potential in an *ab initio* way, which is crucial for determining the true resonances and their resonance parameters. Thus, the resonance at about 2.8 eV in $^1A_1$ component of the one-state CI calculations is not real, and the resonance positions for the two shape resonances $^1A_1$ and $^1B_1$ should be 0.111 and 0.614 eV instead of 0.240 and 0.951 eV, respectively. A test 15-state CI calculation has shown that the two pseudoresonances detected in the one-state CI calculation are washed out as well. The 15-state CI calculations detect the two real shape resonances, but the 22-state CI calculations give much more accurate values of their resonance parameters. It should be noted that the small differences observed between the elastic cross sections of 15-state and 22-state calculations indicate the convergence of coupled-channels results of the present 22-state calculation for the elastic scattering.

Figure 4 shows the four component cross sections (both singlet and triplet), together with the summed elastic integral and Born-corrected cross sections. The $^1A_1$ and $^3A_1$ components play the most important role in the elastic cross sections for the singlet and triplet components, respectively. At the low incident energies, the shape resonances $^1A_1$ and $^1B_1$ contribute the peaks at 0.111 and 0.614 eV, respectively. The Feshbach resonances $^1A_1$ and $^1A_2$ contribute the peaks at 5.832 and 6.802 eV, respectively, which are clearly seen in Fig. 3(a). It should be noted that the $^2a_1$ incident electron interacts with the (first) excited state of $^2B_1$ symmetry, resulting in a threshold effect (round-step) in the $^1B_1$ component at about 1.26 eV, where the $^1B_1$ eigenphase sum is cut short by the excited state $^2B_1$. The other round-steps, or cusps, at about 7.4 eV result also from threshold effects. The Born correction to the integral elastic cross section [see Fig. 4(c)] is very small for the BH_2 radical, except at very low incident energies. This results from the fact that BH_2 has a small static dipole moment and that the Born correction for the rotational $(0 \rightarrow 1)$ component is significant only at very low energies.

The scattering resonances in a multichannel calculation are characterized not only by the mere structures in the cross sections but also, more importantly, by the increase of the eigenphase sum for about π radians in a (generally)

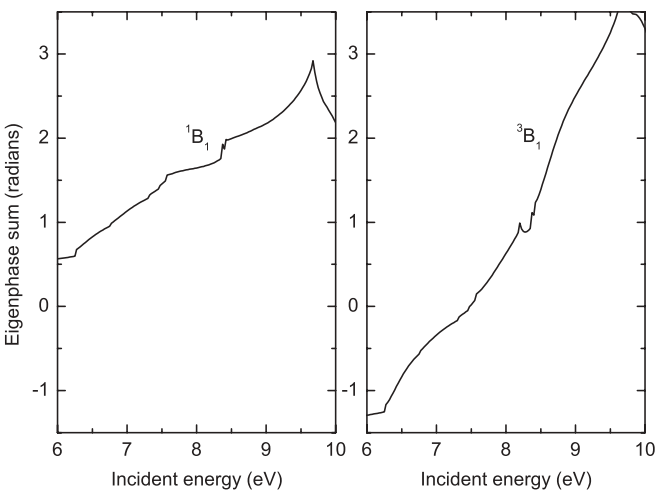

FIG. 5. Eigenphase sum with $^{1,3}B_1$ symmetry for the $N+1$ system in the energy range of 0–10 eV.

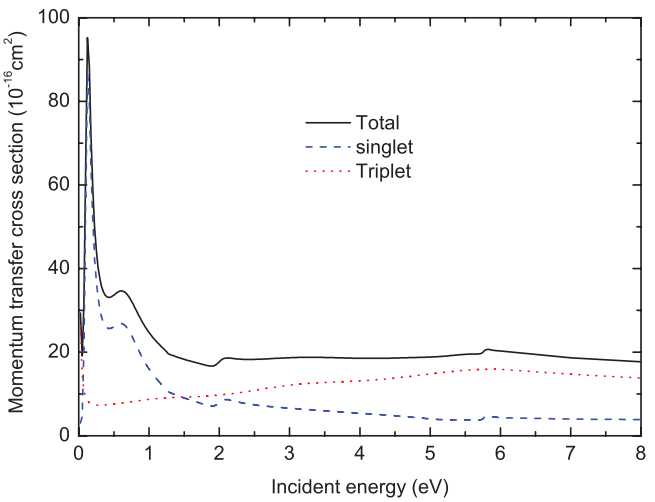

FIG. 6. (Color online) Momentum transfer cross sections in the energy range 0–8 eV.

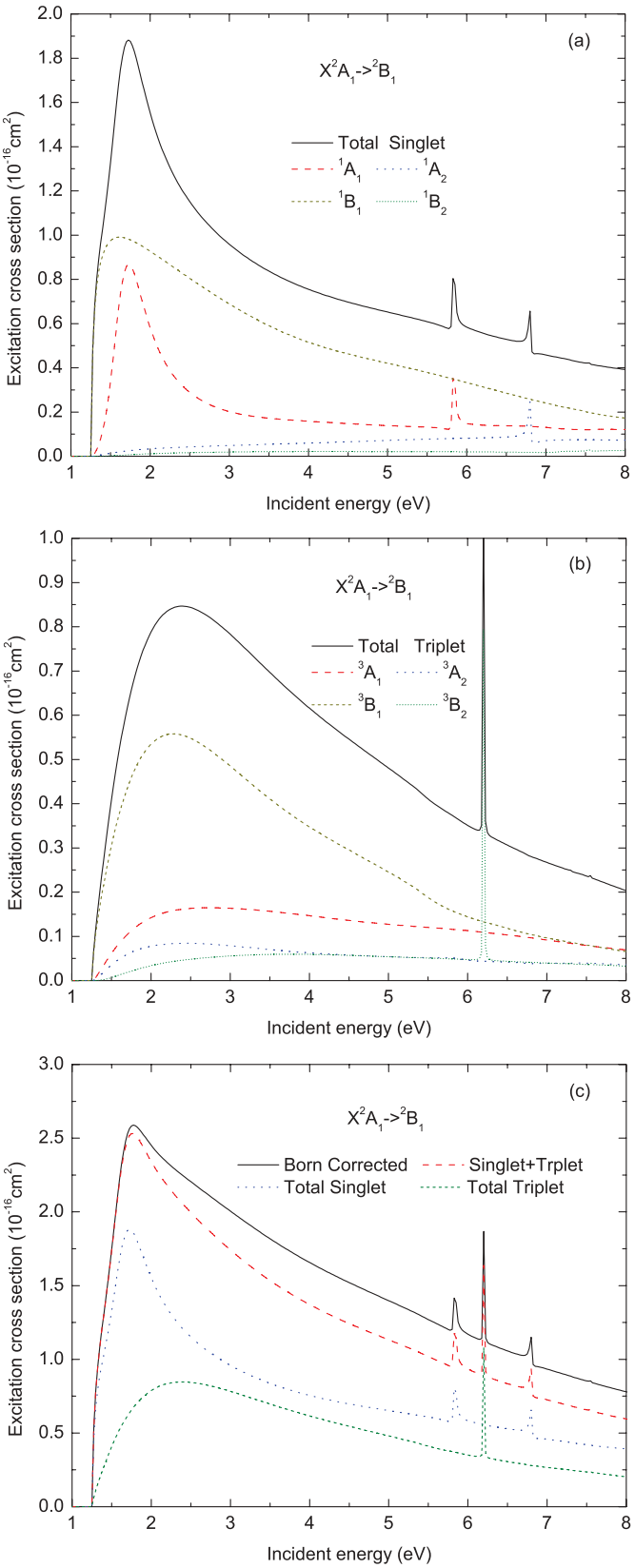

FIG. 7. (Color online) $X\,^2A_1 \rightarrow {}^2B_1$ excitation cross sections in the energy range of 0–8 eV. (a) Singlet A_1, A_2, B_1, and B_2 components and total singlet; (b) triplet A_1, A_2, B_1, and B_2 components and total triplet; (c) total singlet, total triplet, total singlet plus total triplet, and Born corrected.

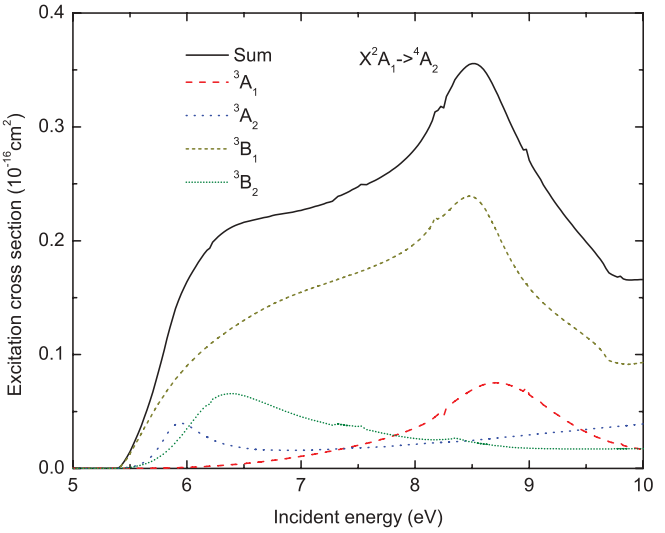

FIG. 8. (Color online) Four triplet components and total for the $X\,^2A_1 \rightarrow {}^4A_2$ excitation cross sections in the energy range of 0–10 eV.

narrow energy range. The resonance parameters (the energy position and the width of the resonance) can (in most cases) be determined by fitting the eigenphase sum to a Breit-Wigner profile [28]. All resonances revealed in the present calculations are presented in Table II, together with the values of their resonance parameters. We should note that since a sparse energy mesh has been employed to produce the cross sections and since the resonance widths of the Feshbach resonances are very narrow, the contributions of these resonances to the total cross sections are very small and are merged in its background. We should also note that several broad resonances between 6 and 10 eV are observed for $^1A_1$ and $^3B_1$, whose eigenphase sums are presented in Fig. 5. It is obvious from this figure that the fitting of these eigenphase sums to a Breit-Wigner profile would lead to large uncertainties in the resonance parameters.

In another open shell molecule, namely NO_2, Munjal *et al.* [29] have found many core-excited shape resonances that result from the large number of valence states in NO_2. The excited spectrum of the BH_2 radical, studied here, is characterized by many both valance and Rydberg states that give rise to several core-excited shape and Feshbach resonances (see Table II). Figure 6 shows the momentum transfer cross section (MTCS), defined as:

$$\sigma_m = 2\pi \int d\sigma/d\Omega(1-\cos\theta)d\theta. \tag{5}$$

MTCS has similar behavior as the integral cross section, but its DCS is not divergent in the forward direction due to the multiplicative factor $(1-\cos\theta)$. It is obvious that the shape resonances $^1A_1$ and $^1B_1$ contribute the peaks at 0.111 and 0.614 eV, respectively, while the small round-step at 5.962 eV originates from the $^3A_2$ core-excited shape resonance.

C. Excitation cross sections

Figures 7 and 8 present the electron impact excitation cross sections from the ground state to the first two excited states $^2B_1$ and $^4A_2$ calculated with our 22-state close-coupling model. According to the dipole selection rules, the transition from the

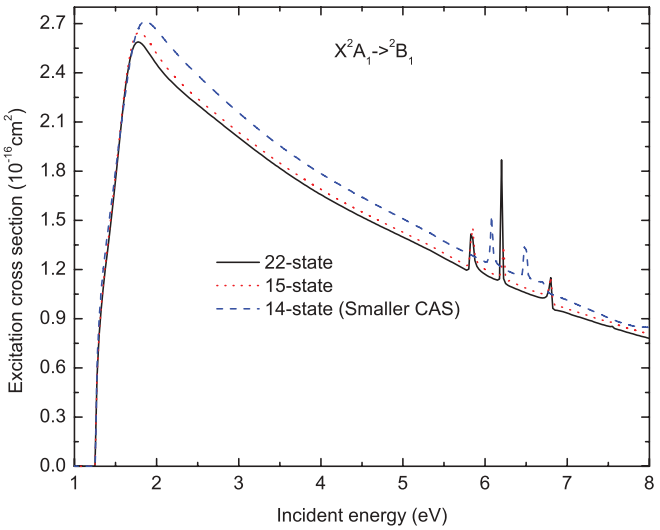

FIG. 9. (Color online) $X\,^2A_1 \rightarrow {}^2B_1$ excitation cross sections for three different models: 22-state, 15-state, and 14-state (with a smaller CAS, see the text for detail information). The 14-state excitation threshold has been shifted lower by 0.047 eV.

ground state X^2A_1 to $^2B_1$ is optically allowed, and the cross section for this transition has been Born corrected [30,31].

The excitation $X\,^2A_1 \rightarrow {}^2B_1$ cross section, which includes four C_{2v} symmetry components (both singlet and triplet), together with their sum and the Born-corrected cross section, are shown in Fig. 7. The large peak in $^1A_1$ at 1.628 eV originates from the $^1A_1$ core-excited shape resonance, while the one at the threshold in $^1B_1$ cross section results from the $^2B_1$ threshold effect. The three Feshbach resonances $^1A_1$,$^3B_2$, and $^1A_2$ clearly manifest themselves in the cross sections as sharp peaks at 5.832, 6.203, and 6.802 eV, respectively. The components $^1B_1$ and $^3B_1$ give the major contributions to the cross sections for this transition in the considered energy range. The triplet components and total excitation cross section for $^4A_2$ excited state are shown in Fig. 8. The shape resonance $^3A_2$ contributes the peak at 5.962 eV, and the broad peaks in $^3A_1$ and $^3B_1$ components result from unresolved broad-width resonances.

Figure 9 shows the $X\,^2A_1 \rightarrow {}^2B_1$ excitation cross sections for three different models. The 22-state and 15-state close-coupling models use the full CAS of present calculations (CAS1: $2a_1-7a_1$,$1b_1$,$2b_1$,$1b_2-4b_2$, and $1a_2$), while 14-state close-coupling model uses a smaller CAS (CAS2: $2a_1-6a_1$, $1b_1$,$2b_1$, and $1b_2-3b_2$). We note that CAS1 produces an excitation threshold smaller by 0.047 eV than that of CAS2, which is closer to the MRD CI result of Ref. [6]. In order to investigate the effect of CAS on the cross section magnitude, we have shifted the threshold of the 14-state close-coupling calculations by 0.047 eV to coincide with that of CAS1. As one can see from Fig. 9, the difference between the cross sections of 14-state and 15-state close-coupling models is quite noticeable (within 5%, except at the resonant energies). The very small difference (less than 1%) between the 15-state and 22-state cross sections indicates that the convergence of the excitation cross section results with respect to the size of coupling channels has been reached. We further note that, as mentioned earlier (see Table I), our CAS1 threshold is higher by about 0.1 eV than the more accurate results of Refs. [3,6]. This threshold energy difference may bring an uncertainty of about 10% in our $X\,^2A_1 \rightarrow {}^2B_1$ excitation cross sections. Generally speaking, a larger basis for B and H and a bigger CAS (or higher CI) would produce more accurate excitation thresholds. However, such a basis and CAS could make the dynamical *R*-matrix calculations intractable.

V. SUMMARY

The present article reports on the results for the elastic differential, integral, momentum transfer, and excitation cross sections for electron impact on BH_2 radical obtained using the 22-state *R*-matrix method with CI target wave functions. This is a detailed *ab initio* study of the low-energy electron scattering on BH_2. The calculations have revealed the presence of four shape and three Feshbach resonances in this scattering system, as well as several broad-width resonances in the energy region 6–10 eV. The threshold energy difference of 0.1 eV between our calculations and those of Ref. [6] may introduce a 10% uncertainty in the $X\,^2A_1 \rightarrow {}^2B_1$ excitation cross section. A similar level of accuracy is expected also for the $X\,^2A_1 \rightarrow {}^4A_2$ excitation cross section. As BH_2 is an important impurity in Tokamak edge and divertor plasmas, the reported cross sections should be valuable in the kinetic studies of these plasmas.

ACKNOWLEDGMENTS

This work was partly supported by the National Natural Science Foundation of China (Grants No. 10734040 and No. 10979007), the National Key Laboratory of Computational Physics Foundation (Grant No. 9140C6904030808), the National Basic Research Program of China (Grant No. 2010CB923301), and the CAS knowledge promotion project (Grant No. KJCX1-YW-N30). One of the authors (S.B.Z.) expresses his gratitude to Dr. Zhe Zhang for his help with the maintenance of the Linux server and to Professor J. Tennyson, Dr. Rui Zhang, and Dr. J. D. Gorfinkiel for their advice and helpful correspondence regarding the use of the molecular *R*-matrix code.

[1] G. Herzberg and J. W. C. Johns, Proc. R. Soc. London A **298**, 142 (1967).
[2] C. F. Bender and H. F. Schaefer III, J. Mol. Spectrosc. **37**, 423 (1971).
[3] V. Staemmler and M. Jungen, Chem. Phys. Lett. **16**, 187 (1972).
[4] G. R. Williams and W. H. Henneker, Mol. Phys. **27**, 1463 (1974).
[5] M. Staikova, M. Peric, and B Engels, J. Mol. Spectrosc. **163**, 221 (1994).
[6] M. Peric, B. Ostojic, and S. D. Peyerimhoff, Z. Phys. D **34**, 241 (1995).
[7] M Kolbuszewski, P. R. Bunker, W. P. Kraemer, G. Osmann, and P. Jensen, Mol. Phys. **88**, 105 (1996).

[8] L. A. Morgan, J. Tennyson, and C. J. Gillan, Comput. Phys. Commun. **114**, 120 (1998).
[9] UK Molecular R-matrix code: [http://www.tampa.phys.ucl.ac.uk/%7Ermat/]
[10] P. G. Burke, I. Mackey, and I. Shimamura, J. Phys. B **10**, 2497 (1977).
[11] P. G. Burke and J. Tennyson, Mol. Phys. **103**, 2537 (2005).
[12] J. Tennyson, Phys. Rep. **491**, 29 (2010).
[13] C. J. Gillan, J. Tennyson, and P. G. Burke, in *Computational Methods for Electron-Molecule Collision*, edited by W. M. Huo and F. A. Gianturo (Plenum, New York, 1995).
[14] J. Tennyson, J. Phys. B **21**, 805 (1988).
[15] G. Herzberg, *Electronic Spectra and Electronic Structure of Polyatomic Molecules* (Van Nostrand, New York, 1966)
[16] T. H. Dunning and P. J. Hay, in *Methods of Electronic Structure Theory*, edited by H. F. Schaefer (Plenum, New York, 1977), Vol. 2.
[17] G. C. Lie and E. Clementi, J. Chem. Phys. **60**, 1275 (1974).
[18] B. N. Plakhutin and E. R. Davidson, J. Phys. Chem. A **113**, 12386 (2009).
[19] J. A. Pople, P. V. R. Schleyer, J. Kaneti, and G. W. Spitznagel, Chem. Phys. Lett. **145**, 359 (1988).
[20] C. J. Cramer, F. J. Dulles, J. W. Storer, and S. E. Worthington, Chem. Phys. Lett. **218**, 387 (1994).
[21] A. Faure, J. D. Gorfinkiel, L. A. Morgan, and J. Tennyson, Comput. Phys. Commun. **144**, 224 (2002).
[22] L. A. Morgan, C. J. Gillan, J. Tennyson, and X. Chen, J. Phys. B **30**, 4087 (1997).
[23] F. A. Gianturco and A. Jain, Phys. Rep. **143**, 347 (1986).
[24] U. Fano and D. Dill, Phys. Rev. A **6**, 185 (1972).
[25] P. G. Burke, N. Chandra, and F. A. Gianturco, J. Phys. B **5**, 2212 (1971).
[26] N. Sanna and F. A. Gianturco, Comput. Phys. Commun. **114**, 142 (1998).
[27] M.-T. Lee, L. E. Machado, L. M. Brescansin, and I. Iga, J. Phys. B **38**, 3795 (2005).
[28] J. Tennyson and C. J. Noble, Comput. Phys. Commun. **33**, 421 (1984).
[29] H. Munjal, K. L. Baluja, and J. Tennyson, Phys. Rev. A **79**, 032712 (2009).
[30] S. I. Chu and A. Dalgarno, Phys. Rev. A **10**, 788 (1974).
[31] S. Kaur, K. L. Baluja, and J. Tennyson, Phys. Rev. A **77**, 032718 (2008).